Inorganic Chemistry

Article

Series of Comparable Dinuclear Group 4 Neo-pentoxide Precursors for Production of pH Dependent Group 4 Nanoceramic Morphologies

Timothy J. Boyle,* Leigh Anna M. Ottley, and Sarah M. Hoppe

Sandia National Laboratories, Advanced Materials Laboratory, 1001 University Boulevard, SE, Albuquerque, New Mexico 87106, United States

Charles F. Campana

5466 East Cheryl Parkway, Madison, Wisconsin 53711, United States

A series of similarly structured Group 4 alkoxides was used to explore the cation effect on the final ceramic nanomaterials generated under different pH solvothermal (SOLVO) conditions. The synthesis of $[Ti(\mu\text{-ONep})(ONep)_3]_2$ (**1**, ONep = $OCH_2C(CH_3)_3$) and $\{[H][(\mu\text{-ONep})_3M_2(ONep)_5(OBu^t)]\}$ where M = Zr (**2**) and Hf (**3**, $OBu^t = OC(CH_3)_3$) were realized from the reaction of $M(OBu^t)_4$ (M = Ti, Zr, Hf) and H-ONep. Crystallization of **1** from py led to the isolation of $[Ti(\mu\text{-ONep})(ONep)_3]_2(\mu\text{-py})$ (**1a**) whereas the dissolution of **2** or **3** in py yielded $\{(\mu_3\text{-O})(\mu_3\text{-OBu}^t)[(\mu\text{-ONep})M(ONep)_2]_3\}$ M = Zr (**2a**) and Hf (**3a**). The structurally similar congener set of **1**–**3** was used to investigate variations of their resultant nanomaterials under solvothermal conditions at high (10 M KOH), low (conc. (aq) HI), and neutral (H_2O) pH conditions. Reproducible nanodots, -squares, and -rods of varied aspect ratios were isolated based on cation and the reaction pH. The hydrolysis products were reasoned to be the "seed" nucleation sites in these processes, and studying the hydrolysis behavior of **1**–**3** led to the identification of $[Ti_6(\mu_3\text{-O})_7(\mu\text{-O})(\mu\text{-ONep})_2(ONep)_6]_2$ (**1b**) for **1** but yielded **2a** and **3a** for **2** and **3**, respectively. A correlation was found to exist between these products and the final nanomaterials formed for the acidic and neutral processes. The basic route appears to be further influenced by another property, possibly associated with the solubility of the final nanoceramic material.

Introduction

Nanomaterials of metal oxide ceramics are being investigated for a wide variety of applications because of the promise of new physical properties expected upon entering this size regime. Of these, group 4 nanoceramics have found widespread use in a diverse array of applications including (i) TiO_2 in photovoltaic and photocatalysis, (ii) ZrO_2 in solid oxide fuel cells and cosmetics, and (iii) HfO_2 in insulator, dielectric, and numerous other electroceramic uses. Reports for the production of TiO_2 nanomaterials (see ref 1 and references therein) are abundant, with fewer routes available for production of ZrO_2 (ref 2–5 are some examples), and

even less for HfO_2 nanoparticles syntheses.[6−8] The majority of these routes focus on the production of nanodots or wires. Recently we reported on the morphological variations noted for TiO_2 "nanoseeds" (i.e., preformed rutile nanoparticles used as nucleation growth sites) processed at high (10 M KOH) and low [(aq)HX; X = Cl, Br, I] pH under solution precipitation (SPPT) and solvothermal (SOLVO) conditions.[1] High aspect ratio nanowires were isolated at high pH while novel nanosquares were observed at low pH.[1]

Molecular precursors to ceramic nanomaterials are of interest since the decomposition of each molecule should be identical, which will lead to similar nucleation events, and thus produce uniform nanomaterials. Further, the thermal stability of metalorganic precursors would be substantially reduced in comparison to a nanoseed process. This could lead

(1) Boyle, T. J.; Lambert, T. N.; Pratt, H. D. I.; Lu, P.; Griego, J. J. M.; Bush, N.; Chavez, C. A.; Welk, M. *J. Mater. Sci.* **2010**, *45*, 1744.
(2) Karthikeyan, J.; Berndt, C. C.; Tikkaanen, J.; Wang, J. Y.; King, A. H.; Herman, H. *Nanostruct. Mater*. **1997**, *8*, 61.
(3) Burakorn, T.; Panpranot, J.; Mekasuwandumrong, O. *J. Mater. Process. Technol.* **2008**, *206*, 352.
(4) Battez, A. H.; Gonzalez, R.; Viesca, J. L. *Wear* **2008**, *265*, 422.
(5) Chaubey, G. S.; Kim, J. *Bull. Korean Chem. Soc.* **2007**, *28*, 2279.
(6) Maikap, S.; Das, A.; Want, T. Y.; Tien, T. C.; Chang, L. B. *J. Electrochem. Soc.* **2009**, *156*, K28.
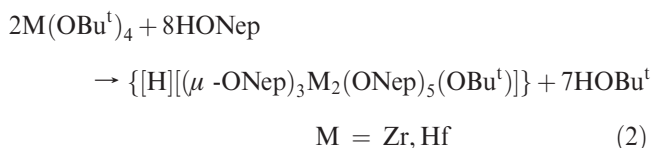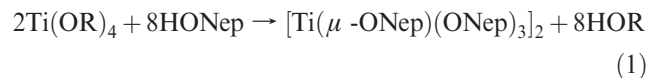(7) Lin, Y. H.; Chien, C. H.; Lin, C. T.; Chang, C. Y.; Lei, T. F. *IEEE Trans. Electron Devices* **2006**, *53*, 782.
(8) Das, A.; Maikap, S.; Li, W.-C.; Chang, L.-B.; Yang, J.-R. *Jpn. J. Appl. Phys.* **2009**, *48*, 05DF02.

to lower processing temperatures impacting a number of advanced ceramic systems. Additionally, it is of interest to understand how the cations and their associated chemistry affect the final nanomaterial properties. To meaningfully accomplish this goal, it is critical to have similar shaped precursors for a group to minimize the variables in the reaction process. Unfortunately, this uniformity is not common for metal alkoxides $(M(OR)_x)$.[9−11]

One of the most useful alkoxide ligands that we have found[12−32] for materials synthesis is the *neo*-pentoxide $(OCH_2C(CH_3)_3$ or ONep) moiety. The ONep ligand is attractive since it often yields compounds with reduced oligomerization and thus higher solubility and/or volatility, low decomposition temperatures with low C retention, minimal side reactions, and ease of crystallization, critical for identification of $M(OR)_x$. Over a decade ago, the synthesis of $[Ti(\mu\text{-}ONep)(ONep)_3]_2$ (**1**) from the alcoholysis of $Ti(OPr^i)_4$ (where $OPr^i = OCH(CH_3)_2$) with 4 equiv HONep in toluene (eq 1) was reported.[33] Subsequently, extensive investigations of **1** for both chemical and materials production have been reported.[12−31] Our previous attempts to extend this chemistry to Zr resulted only in partial substitution or oxo formation.[31]

Since these initial reports, no additional homoleptic ONep Group 4 structures have been disseminated.[9−11]

$$2Ti(OR)_4 + 8HONep \rightarrow [Ti(\mu\text{-}ONep)(ONep)_3]_2 + 8HOR \tag{1}$$

$$2M(OBu^t)_4 + 8HONep$$

$$\rightarrow \{[H][(\mu\text{-}ONep)_3M_2(ONep)_5(OBu^t)]\} + 7HOBu^t$$

$$M = Zr, Hf \tag{2}$$

Recently, interest in generating the homoleptic ONep congeners led to the study of the *tert*-butoxide $(OC(CH_3)_3$ or $OBu^t)$ derivatives as shown in eq 2. The products were eventually characterized as $\{[H][(\mu\text{-}ONep)_3M_2(ONep)_5(OBu^t)]\}$ M = Zr (**2**) and Hf (**3**) with a proton disordered over the entire molecule. The surprisingly similar dinuclear structure types observed for these congeners (**1−3**) allows for a comparative investigation of the influence of the metal cation on the final ceramic materials' properties under low, neutral, and high pH conditions following established solvothermal (SOLVO) routes.[33] The characterization of the starting materials (**1−3**), the pyridine adducts $\{[Ti(\mu\text{-}ONep)(ONep)_3]_2\text{-}(\mu\text{-}py)$ [**1a**], **2a**, and **3a**], and hydrolysis products $[Ti_6(\mu_3\text{-}O)_7(\mu\text{-}O)(\mu\text{-}ONep)_2(ONep)_6]_2$ [(**1b**), **2a**, **3a**], and the final nanomaterials generated by these unusual similarly shaped group 4 precursors are reported.

Experimental Section

All compounds described below were handled under an argon atmosphere with rigorous exclusion of air and water using standard Schlenk line and glovebox techniques. All solvents were stored under argon and used as received (Aldrich) in Sure/Seal bottles, including toluene (tol) and pyridine (py). The following chemicals were used as received (Aldrich and Alfa Aesar): $M(OBu^t)_4$ (M = Ti, Zr, Hf) and H-ONep. $Ti(OPr^i)_4$ was freshly distilled prior to use. Compound **1** was prepared according to literature procedures[33] and from the reaction of $Ti(OBu^t)_4$ with 4.5 HONep in toluene.

FT-IR data were obtained on a Bruker Vector 22 Instrument using KBr pellets under an atmosphere of flowing nitrogen. Elemental analysis was performed on a Perkin-Elmer 2400 CHN-S/O Elemental Analyzer. All NMR samples were prepared from dried crystalline materials that were handled and stored under an argon atmosphere and redissolved in deuterated chloroform $(CDCl_3)$. Spectra were collected on a Bruker DRX 400 MHz NMR spectrometer under standard experimental conditions (^1H spectra 4-s recycle delay at 16 scans; ^13C Spectra were obtained with a 10 s delay and 4k scans).

$\{[H][(\mu\text{-}ONep)_3Zr_2(ONep)_5(OBu^t)]\}$ (**2**). To a stirring solution of $Zr(OBu^t)_4$ (1.00 g, 2.61 mmol), in ~10 mL of toluene, H-ONep (1.03 g, 11.7 mmol), was added. After 12 h, a precipitate was present, the reaction was heated until clear and set aside until crystals formed. Yield 92.7% (1.15 g). FTIR (KBr Pellet, cm^{-1}) 3440(br, m), 2954(s), 2908(s), 2867(w), 1651(w), 1478(m), 1395(m), 1363(m), 1261(w), 1194(s), 1135(s), 1111(s), 1017(s), 1017(w), 904(w), 800(w), 751(w), 630(m), 580(w), 533(w), 457(m). ^1H NMR (400.1 MHz, CDCl_3) δ 3.98 (14.0H, s, OCH_2C(CH_3)_3$), 1.32 (5.8H, s, OC(C$H_3$)_3$), 1.07 (62.6H, s, OCH_2C(CH_3)_3$). ^13C (100.1 MHz, CDCl_3) δ 80.1 (OCH_2C(CH_3)_3$), 33.6 (O$C$(CH_3)_3$), 32.8 (OCH_2C(CH_3)_3$), 27.0 (OCH_2C($C$H_3)_3$). Elemental Analysis $C_{44}H_{98}O_9Zr_2$ (MW = 953.69): calc'd 55.41, % C; 10.36, %H. Found 55.58, %C; 10.64, %H.

(9) Allen, F. H.; Bellard, S.; Brice, M. D.; Cartwright, B. A.; Doubleday, A.; Higgs, H.; Hummelink, T.; Hummelink-Peters, B. G.; Kennard, O.; Motherwell, W. D. D.; Rodgers, J. R.; Watson, D. G. *Acta Crystallogr.* **1979**, *B35*, 146.

(10) Allen, F. H.; Kennard, O.; Taylor, R. *Acc. Chem. Res.* **1983**, *16*, 146.

(11) Cambridge Crystallographic Data Centre, 12 Union Road, Cambridge CB2 1EZ, United Kingdom; www.ccdc.cam.ac.uk; searched using ConQuest v 5.31 (Nov 2009).

(12) Boyle, T. J.; Alam, T. M.; Bunge, S. D.; Segall, J. M.; Avilucea, G. R.; Tissot, R. G.; Rodriguez, M. A. *Organometallics* **2005**, *24*, 731.

(13) Boyle, T. J.; Alam, T. M.; Dimos, D.; Moore, G. J.; Buchheit, C. D.; Al-Shareef, H. N.; Mechenbier, E. R.; Bear, B. R.; Ziller, J. W. *Chem. Mater.* **1997**, *9*, 3187.

(14) Boyle, T. J.; Alam, T. M.; Peters, K. P.; Rodriguez, M. A. *Inorg. Chem.* **2001**, *40*, 6281.

(15) Boyle, T. J.; Alam, T. M.; Rodriguez, M. A.; Zechmann, C. A. *Inorg. Chem.* **2002**, *41*, 2574.

(16) Boyle, T. J.; Alam, T. M.; Tafoya, C. J.; Mechenbier, E. R.; Ziller, J. W. *Inorg. Chem.* **1999**, *38*, 2422.

(17) Boyle, T. J.; Alam, T. M.; Tafoya, C. J.; Scott, B. L. *Inorg. Chem.* **1998**, *37*, 5588.

(18) Boyle, T. J.; AlShareef, H. N. *J. Mater. Sci.* **1997**, *32*, 2263.

(19) Boyle, T. J.; Andrews, N. L.; Alam, T. M.; Rodriguez, M. A.; Santana, J. M.; Scott, B. L. *Polyhedron* **2002**, *21*, 2333.

(20) Boyle, T. J.; Andrews, N. L.; Rodriguez, M. A.; Campana, C.; Yiu, T. *Inorg. Chem.* **2003**, *42*, 5357.

(21) Boyle, T. J.; Bunge, S. D.; Alam, T. M.; Holland, G. P.; Headley, T. J.; Avilucea, G. *Inorg. Chem.* **2005**, *44*, 1309.

(22) Boyle, T. J.; Bunge, S. D.; Andrews, N. L.; Matzen, L. E.; Sieg, K.; Rodriguez, M. A.; Headley, T. J. *Chem. Mater.* **2004**, *16*, 3279.

(23) Boyle, T. J.; Ottley, L. A. M.; Brewer, L. N.; Sigman, J.; Clem, P. G.; Richardson, J. J. *Eur. J. Inorg. Chem.* **2007**, 3805.

(24) Boyle, T. J.; Ottley, L. A. M.; Daniel-Taylor, S. D.; Tribby, L. J.; Bunge, S. D.; Costello, A. L.; Alam, T. M.; Gordon, J. C.; McCleskey, T. M. *Inorg. Chem.* **2007**, *46*, 3705.

(25) Boyle, T. J.; Ottley, L. A. M.; Rodriguez, M. A. *Polyhedron* **2005**, *24*, 1727.

(26) Boyle, T. J.; Pedrotty, D. M.; Scott, B.; Ziller, J. W. *Polyhedron* **1998**, *17*, 1959.

(27) Boyle, T. J.; Rodriguez, M. A.; Alam, T. M. *Dalton Trans.* **2003**, 4598.

(28) Boyle, T. J.; Schwartz, R. W. *Comments Inorg. Chem.* **1994**, *16*, 243.

(29) Boyle, T. J.; Tyner, R. P.; Alam, T. M.; Scott, B. L.; Ziller, J. W.; Potter, B. G. *J. Am. Chem. Soc.* **1999**, *121*, 12104.

(30) Boyle, T. J.; Ward, T. L.; De'Angeli, S. M.; Xu, H. F.; Hammetter, W. F. *Chem. Mater.* **2003**, *15*, 765.

(31) Boyle, T. J.; Gallegos, J. J.; Pedrotty, D. M.; Mechenbier, E. R.; Scott, B. L. *J. Coord. Chem.* **1999**, *47*, 155.

(32) Boyle, T. J.; Tribby, L. J.; Bunge, S. D. *Eur. J. Inorg. Chem.* **2006**, 4553.

(33) Boyle, T. J.; Alam, T. M.; Mechenbier, E. R.; Scott, B. L.; Ziller, J. W. *Inorg. Chem.* **1997**, *36*, 3293.

Table 1. Data Collection Parameters for **1–3**

	$\mathbf{1}$[33]	$\mathbf{1a}$	$\mathbf{1b}$	$\mathbf{2}$	$\mathbf{2a}$	$\mathbf{3}$	$\mathbf{3a}$
chemical formula	$C_{40}H_{88}O_8Ti_2$	$C_{45}H_{93}NO_8Ti_2$	$C_{80}H_{176}O_{32}Ti_{12}$	$C_{45}H_{99}O_9Zr_2$	$C_{49}H_{108}O_{11}Zr_3$	$C_{45}H_{99}Hf_2O_9$	$C_{98}H_{216}Hf_6O_{22}$
formula weight	792.90	872.00	2225.01	966.68	1147.01	1141.22	2817.65
temp (K)	188	173(2)	173(2)	173(2)	173(2)	173(2)	173(2)
space group	triclinic $P\bar{1}$	monoclinic $C2/c$	triclinic $P\bar{1}$	monoclinic $P2(1)$	trigonal $P3c\bar{1}$	monoclinic $P2(1)$	trigonal, $P3c\bar{1}$
a (Å)	11.608(3)	25.978(4)	15.0128(9)	10.7608(15)	18.9319(16)	10.7521(17)	18.867(3)
b (Å)	12.308(7)	10.0771(15)	15.5671(10)	18.481(3)	18.9319(16)	18.481(3)	18.867(3)
c (Å)	19.752(4)	21.138(3)	15.8982(10)	14.522(2)	23.033(3)	14.477(2)	23.072(9)
α	83.36		65.9560(10)				
β (deg)	76.34	108.869(2)	61.9040(10)	105.945(2)		105.692(2)	
γ	62.14		89.4420(10)		120		120
V (Å^3)	2424.29	5236.1(13)	2909.8(3)	2776.9(7)	7149.4(12)	2769.5(8)	7112.3(10)
Z	2	4	1	2	4	2	2
D_{calcd} (Mg/m^3)	1.086	1.106	1.270	1.156	1.066	1. 369	1.316
μ,(Mo, Kα) (mm^{-1})	0.371	0.350	0.838	0.419	0.470	3.789	4.409
R1^a (%) (all data)	7.56 (16.29)	8.32(9.43)	6.95(8.43)	10.97(12.14)	4.29(4.52)	4.87(6.54)	3.97(3.53)
wR2^b (%) (all data)	14.16 (18.27)	19.26(20.00)	17.76(18.67)	34.15(37.93)	11.69(11.84)	12.30(13.61)	7.88(8.11)

^{a} R1 = $\sum||F_o| - |F_c||/\sum|F_o| \times 100$. ^{b} wR2 = $[\sum w(F_o^2 - F_c^2)^2/\sum w(F_o^2)^2]^{1/2} \times 100$.

$\{[H][(\mu\text{-ONep})_3Hf_2(\text{ONep})_5(\text{OBu}^t)]\}$ (**3**). To a stirring solution of Hf(OBu^t)$_4$ (1.00 g, 2.12 mmol) in ~10 mL of toluene, H-ONep (0.841 g, 9.56 mmol) was added. After 12 h, a precipitate was present, the reaction was heated until clear and set aside until crystals formed. Yield 73.3% (0.88 g). FTIR (KBr Pellet, cm^{-1}) 3577(br,m), 2953(s), 2866(s), 2708(m), 1479(m), 1396(m), 1363(m), 1261(w), 1149(s), 1123(s), 1041(sh), 1016-(sm), 937(w), 902(w), 752(w), 626(m), 583(w), 536(w), 450(m). ^{1}H NMR (400.1 MHz, CDCl$_3$) δ 4.06 (14.0H, s, OCH_2C-(CH$_3$)$_3$), 1.32 (8.4H, s, OC(CH_3)$_3$), 1.07 (67.5H, s, OCH$_2$C-(CH_3)$_3$). ^{13}C (100.1 MHz, CDCl$_3$) δ 79.9 (OCH$_2$C(CH$_3$)$_3$), 33.7 (OC(CH$_3$)$_3$), 32.9 (OCH$_2$$C$(CH$_3$)$_3$), 27.1 (OCH$_2$C($CH_3$)$_3$). Elemental Analysis for C$_{44}$H$_{98}$Hf$_2$O$_9$ (MW = 1128.23): calc'd 46.84, %C; 8.75, %H. Found 46.49, %C; 8.96, %H.

Pyridine Adducts. Under an atmosphere of argon, the above crystalline material (**1–3**) was dissolved in a minimum amount of pyridine with heating if necessary. The resulting crystals isolated in near quantitative yields were characterized by single crystal diffraction as [Ti(μ-ONep)(ONep)$_3$]$_2$(μ-py) (**1a**) and $\{(\mu_3\text{-O})(\mu_3\text{-OBu}^t)[(\mu\text{-ONep})M(\text{ONep})_2]_3\}$ where M = Zr (**2a**) and Hf (**3a**).

Hydrolysis Products. To a solution of the crystalline material of **1–3** independently dissolved in a minimum amount of toluene, 1 equiv of water in toluene was cannula transferred from one Schlenk flask to another. The final reaction mixture was stirred for 5 min and then all the volatile materials removed in vacuo to yield white powders. The products were transferred to a glovebox and crystallized from toluene. The products were identified as [Ti$_6$(μ_3-O)$_7$(μ-O)(μ-ONep)$_2$(ONep)$_6$]$_2$ (**1b**) whereas **2** and **3** yielded **2a** and **3a**, respectively.

Beryllium X-ray Powder Patterns (BeD-XRD). Information pertaining to the details of the beryllium dome XRD (BeD-XRD) analyses has been previously disseminated;[34–36] hence, only a short description is presented here. All sample preparation was performed in an argon filled glovebox using a 1 cm quartz disk (zero-background plate), where the sample was pressed into the specimen cavity, leveled to the holder base using a glass slide, and the BeD cover sealed. The BeD holder was carefully loaded into the Siemens D500 diffractometer. For all scans the instrument settings were 40 kV and 30 mA with a 0.04° step-size, 1 s count-time, scan range of 5–30° 2θ, 1° divergence and receiving slits; the goniometer radius was 250 mm. *Caution! Because of the presence of potentially toxic Be^o, it is important that only trained personnel, wearing the appropriate personal protective equipment (i.e., rubber gloves) handle the BeD. If poor handling techniques or any other means shatter the BeD, proper safety cleanup and disposal protocols* **must** *be followed.*

General X-ray Crystal Structure Information.[37] Crystals were mounted onto a glass fiber from a pool of Fluorolube and immediately placed in a cold N$_2$ vapor stream, on a Bruker AXS diffractometer equipped with a SMART 1000 CCD detector using graphite monochromatized MoKα radiation (λ = 0.7107 Å). Lattice determination and data collection were carried out using SMART Version 5.054 software. Data reduction was performed using SAINTPLUS Version 6.01 software and corrected for absorption using the SADABS program within the SAINT software package.

Structures were solved by direct methods that yielded the heavy atoms, along with a number of the lighter atoms or by using the PATTERSON method, which yielded the heavy atoms. Subsequent Fourier refinement yielded the remaining light-atom positions. The hydrogen atoms were fixed in positions of ideal geometry and refined using SHELXH software. The final refinement of each compound included anisotropic thermal parameters for all non-hydrogen atoms. It is of note that crystal structures of M(OR)$_x$ often contain disorder within the atoms of the ligand chain causing higher than normal final correlations.[38–43] All final CIF files were checked at http://www.iucr.org/. Additional information concerning the data collection and final structural solutions can be found in the Supporting Information or by accessing CIF files through the Cambridge Crystallographic Data Base. Data collection parameters for **1–3a** are given in Table 1. Specific issues associated with individual structures are discussed below.

Compounds **2** and **3** have isomorphous structures and both were solved and refined in the monoclinic space group $P2_1$ with Z = 2. Nearly perfect inversion twinning was observed for both compounds with refined twin ratios of 0.486 and 0.507 for **2** and **3**, respectively. The atoms of the core M$_2$O$_9$ units were refined anisotropically, while the carbon atoms of the nine *neo*-pentoxide ligands were refined isotropically. All methylene and

(34) Boyle, T. J.; Ottley, L. A. M.; Alam, T. M.; Rodriguez, M. A.; Yang, P.; McIntyre, S. K. *Polyhedron* **2010**, *29*, 1784.

(35) Rodriguez, M. A.; Boyle, T. J.; Yang, P.; Harris, D. L. *Powder Diffr.* **2008**, *23*, 121.

(36) Boyle, T. J.; Ottley, L. A. M.; Rodriguez, M. A.; Sewell, R. M.; Alam, T. M.; McIntyre, S. K. *Inorg. Chem.* **2008**, *47*, 10708.

(37) Turova, N. Y.; Turevskaya, e. P.; Kessler, V. G.; Yanovskay, M. L. *The Chemistry of Metal Alkoxides*; Kluwer Academic Publishers: Boston, 2002.

(38) Bradley, D. C.; Mehrotra, R. C.; Gaur, D. P. *Metal Alkoxides*; Academic Press: New York, 1978.

(39) Bradley, D. C.; Mehrotra, R. C.; Rothwell, I. P.; Singh, A. *Alkoxo and Aryloxo Derivatives of Metals*; Academic Press: New York, 2001.

(40) Turova, N. Y.; Turevskaya, E. P.; Kessler, V. G.; Yanovskaya, M. I. *The Chemistry of Metal Alkoxide*; Kluwer Academic Publishers: Boston, 2002.

(41) Caulton, K. G.; Hubert-Pfalzgraf, L. G. *Chem. Rev.* **1990**, *90*, 969.

(42) Chandler, C. D.; Roger, C.; Hampden-Smith, M. *J. Chem. Rev.* **1993**, *93*, 1205.

(43) Hubert-Pfalzgraf, L. G. *New. J. Chem.* **1987**, *11*, 663.

methyl hydrogen atoms were placed in idealized positions and refined as using a riding model. Careful examination of the raw image data from the CCD detector revealed that both structures are commensurate modulated structures with q-vector of 0, 0, 1/3, with the intensities of the satellite peaks in compound **2** being much larger than those in compound **3**. The structures reported in this work are based upon the small subcell and do not include the contributions due to the satellite reflection. These structures are therefore average structures, which have larger than expected isotropic displacement parameters for the carbon atoms, and unusually high R-values of R1 = 10.97% for **2** and 4.29% for **3**. The experimental data were not of sufficiently good quality to attempt a complete modulated structure analysis.

Compounds **2a** and **3a** have isomorphous structures, and both were solved and refined in the trigonal space group $P3c\overline{1}$ with $Z = 2$. Each of molecules lies on a crystallographic 3-fold axis. One of the *neo*-pentoxide ligands is disordered and was successfully refined using standard crystallographic restraints. The disorder ratios refined to 0.423 and 0.350 for **2a** and **3a**, respectively. The carbon atoms of the disordered ligands were refined isotropically, and all other non-hydrogen atoms were refined anisotropically. All methylene and methyl hydrogen atoms were placed in idealized positions and refined as using a riding model.

Nanoparticle Synthesis. Compounds **1−3** were used in three solutions under SOLVO conditions (in a 40 mL Parr Digestion bomb, 1.2 mmol of precursor, 20 mL total, heated to 180 °C for 24 h) that involves the addition of the desired precursor to a solution at a variety of pH levels: (a) low [*conc.* HI/H_2O (1:1)], (b) neutral (H_2O), and (c) high (10 M (aq) KOH). After the appropriate time, the precipitate was isolated by centrifugation and washed with water three times.

For transmission electron microscopy (TEM) analyses, an aliquot of the desired powder that was slurried in toluene was placed directly onto a holey-carbon copper coated TEM grid (300 mesh) purchased from Electron Microscopy Sciences and allowed to dry overnight. The resultant particles were studied using a Philips CM 30 TEM operating at 300 kV accelerating voltage. In addition, the powder was characterized using a PANalytical X'Pert Pro using Cu Kα radiation with step size 0.0167 degree, with 0.152 deg/sonds dwelling time. The nanoceramic sample was placed on a zero background XRD holder, which minimized the background noise on XRD signal.

Results and Discussion

Since the reports on the synthesis of **1** (shown in Figure 1), only a handful of other Group 4 ONep derivatives have been crystallographically characterized,[9−11] including [Zr(μ-OPr^i)(ONep)$_3$(HONep)]$_2$,[31] [Zr$_3$(μ_3-O)(μ_3-ONep)(μ-ONep)$_3$-(ONep)$_6$],[31] and Zr(O)(Cl)(μ-ONep)$_3$(ONep)$_6$.[44] The Hf(OR)$_4$
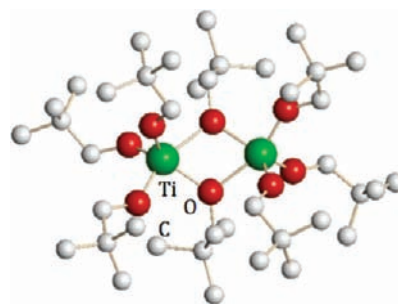

Figure 1. Ball and stick structure plot of **1**.[22]

family has only been cursorily investigated[45−53] and no Hf-ONep derivatives have been previously reported. While these compounds have interesting and useful properties, they did not allow for a systematic investigation of the cation effect on the subsequent materials produced. For instance, zirconium based alkoxides are classically thought to be very stable dinuclear species with the central Zr-OPr^i core known to be chemical resistant, with a number of researchers actually using [Zr(μ-OPr^i)(OPr^i)(HOPr^i)]$_2$ as a ligand.[37−39,42,43,54−60] Thus, the heteroleptic [Zr(μ-OPr^i)(ONep)$_3$(HONep)]$_2$ with a "Zr$_2$(μ-OPr^i)$_2$" core[31] would not be of use in comparison to **1** with a "M$_2$(μ-ONep)$_2$". Therefore, it was of interest to generate a series of similar ligated, dinuclear Group 4 congener species and investigate the effect the cation had on the final nanomaterials generated.

Synthesis. The reaction of the monomeric Zr(OBu^t)$_4$ with stoichiometric amounts of HONep produced no color change nor any precipitate upon mixing. After stirring for 12 h, crystals were easily isolated by drastically reducing the volume of the reaction mixture and allowing the solution to set for several hours under an inert atmosphere. Because of the success with the Zr(OBu^t)$_4$, Hf-(OBu^t)$_4$ was reacted in a similar process as noted above. The crystals isolated from a variety of solvents: hexanes, toluene, and CHCl$_3$.

Single Crystal X-ray. To assist in identification of the products, single crystal X-ray diffraction experiments were undertaken. While the crystals isolated from toluene or hexanes yielded a structural solution, their final models suffered from significant disorder in ligands' pendant hydrocarbon chains, yielding high R-values, not uncommon for M(OR)$_x$ structure solutions.[38−43] The best-fit structure solutions of **2** and **3** were ultimately obtained from crystals grown from CHCl$_3$ and are shown in Figures 2 and 3, respectively. Irrespective of the extensive modeling efforts undertaken, disorder in the ONep ligands was observed. However, the central core of **2** and **3** was unequivocally determined to be dinuclear with 9 ONep

(44) Evans, W. J.; Ansari, M. A.; Ziller, J. W. *Polyhedron* **1998**, *17*, 869.

(45) Sarikove, Z. A.; Turevskaya, E. P.; Kozlova, N. I.; Turova, N. Y.; Berdyev, D. V.; Anovsky, A. I. *Polyhedron* **1999**, *18*, 941.

(46) Chmura, A. H.; Davidson, M. G.; Jones, M. D.; Lunn, M. D.; Mahon, M. F.; Johnson, A. F.; Khunkamchoo, P.; Roberts, S. L.; Wong, S. S. F. *Macromolecules* **2006**, *39*, 7250.

(47) Williams, P. A.; Roberts, J. L.; Jones, A. C.; Chalker, P. R.; Tobin, N. L.; Bickley, J. F.; Davies, H. O.; Smith, L. N.; Leedham, T. J. *Chem. Vap. Deposition* **2002**, *8*, 163.

(48) Boyle, T. J.; Tribby, L. J.; Alam, T. M.; Bunge, S. D.; Holland, G. P. *Polyhedron* **2005**, *24*, 1143.

(49) Veith, M.; Mathur, S.; Mathur, C.; Huch, V. *J. Chem. Soc., Dalton Trans.* **1997**, *12*, 2101.

(50) Loo, Y. F.; O'kane, R.; Jones, A. C.; Aspinall, H. C.; Potter, R. J.; Chalker, P. R.; Bickley, J. F.; Taylor, S.; Smith, L. M. *J. Mater. Chem.* **2005**, *15*, 1896.

(51) Chmura, A. H.; Davidson, M. G.; Jones, M. D.; Lunn, M. D.; Mahon, M. F. *Dalton Trans.* **2006**, *7*, 887.

(52) Williams, P. A.; Roberts, J. L.; Jones, A. C.; Chalker, P. R.; Bickley, J. F.; Steiner, A.; Davies, H. O.; Leedham, T. J. *J. Mater. Chem.* **2002** *12*, 165.

(53) Imam, S. A.; Rao, B. R. *Naturwissenschaften* **1963**, *50*, 517.

(54) Bradley, D. C. *Chem. Rev.* **1989**, *89*, 1317.

(55) Cotton, F. A.; Wilkinson, G. *Advanced Inorganic Chemistry*, 5th ed.; John Wiley & Sons: New York, 1988.

(56) Veith, M.; Mathur, S.; Huch, V.; Decker, T. *Eur. J. Inorg. Chem.* **1998**, *9*, 1327.

(57) Veith, M.; Mathur, C.; Mathur, S.; Huch, V. *Organometallics* **1997**, *16*, 1292.

(58) Evans, W. J.; Greci, M. A.; Ansari, M. A.; Ziller, J. W. *J. Chem. Soc., Dalton Trans.* **1997**, *23*, 4503.

(59) Evans, W. J.; Johnston, M. A.; Ansari, M. A.; Brady, J. C.; Ziller, J. W. *Inorg. Chem.* **2000**, *39*, 2125.

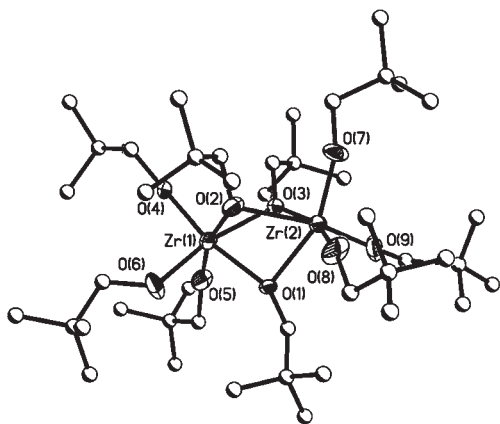(60) Evans, W. J.; Greci, M. A.; Johnston, M. A.; Ziller, J. W. *Chem.—Eur. J.* **1999**, *5*, 3482.

Figure 2. Structure plot of **2**. Thermal ellipsoids drawn at the 30% level of heavy atoms.
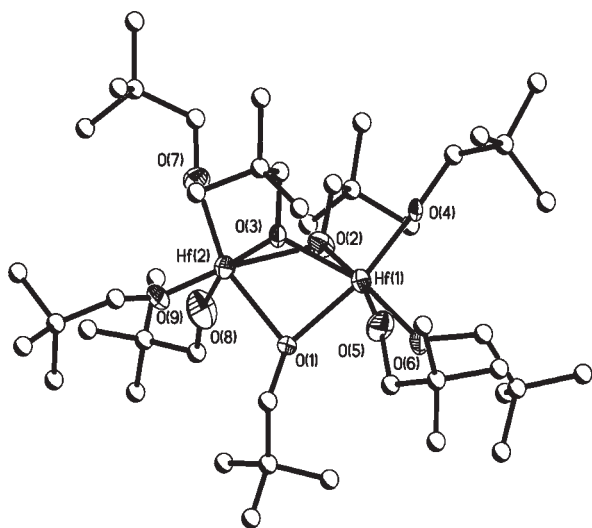

Figure 3. Structure plot of **3**. Thermal ellipsoids drawn at the 30% level of heavy atoms.

ligands: 3 bridging and 6 terminal yielding octahedral geometries for each metal center. To maintain charge balance, one of the 9 ONep ligands must be protonated; however, the location of the H could not be discerned from an analysis of the metrical data nor the electron density map. Therefore, it was assumed that the proton was disordered over the entire molecule and represented by a [H] in the formula. The metrical data are shown in Table 2 and were found to be consistent with each other when the cation size variation is taken into account.

Bulk Powder Characterization. The bulk crystalline powder was further characterized using a variety of analytical methods. The FTIR spectrum of the crystals of **2** or **3** contained standard ONep stretches and bends; however, even when carefully dried and handled, a substantial OH peak was observed around 3400 cm^{-1} for each sample. This is consistent with the disordered H assumed in the crystal structure (vide infra). The sharp stretches noted at 630 and 450 cm^{-1} for **2** and at 626 and 457 cm^{-1} for **3** correspond to the various M−O bonds. The remaining peaks in these two spectra are nearly identical, suggesting that the two species possess similar constructs, as noted in their single crystal structures.

Elemental analysis of **1** has always proved problematic because of the volatility of the precursor, which melts

at 59 °C. For **2** and **3**, the samples were found to melt at 210 and 181 °C, respectively which indicated that useful analyses might be obtained. Elemental analyses of **2** and **3** proved to be consistent with the above single crystal structure solutions.

Alternative methods were also undertaken to confirm that the bulk powders were consistent with the single crystal structure. The use of a beryllium dome XRD (BeD-XRD) for analysis of air-sensitive materials has been shown to be an important method to identify highly reactive powders.[35,36] The resultant BeD-XRD spectra of **1**−**3** were in agreement with the calculated patterns of **1**−**3** that were derived from the single crystal structure, and these data can be found in the Supporting Information. Combined, the above data suggested that the full structure was the homoleptic ONep dinuclear complex.

Pyridine Derivatives. One final attempt to generate higher quality crystals led to isolating crystals from pyridine. For **1**, the sample rapidly dissolved in a minimum amount of pyridine whereas reaction mixtures of both **2** and **3** had to be heated to obtain clear solutions. The crystals isolated upon cooling of the reaction mixture of **1**, **2**, and **3** proved to be [Ti(μ-ONep)(ONep)$_3$]$_2$(μ-py) (**1a**, Figure 4) and a surprising {(μ_3-O)(μ_3-OBu^t)[(μ-ONep)M(ONep)$_2$]$_3$} M = Zr (**2a**, Figure 5) and Hf (**3a**, Figure 6).

For **1a**, the pyridine molecule was located in a bridging position between the two metal centers; however, the Ti−N distance is too elongated [2.532(8) Å] to be considered a full bond (literature Ti−N(py) distances range from 2.141−2.455 Å)[9−11] and more likely represents a weak interaction. This so-called "crevice" binding mode has only been noted for three other compounds {[(C$_6$-H$_{11}$)$_3$P]Ag(μ-I)}$_2$(μ-py),[61] {[CsP(H)(C$_6$H$_2$Bu^t$_3$)-2,4,6]$_2$-(μ-py),[62] and {(L)$_2$Mo(O)]$_2$(μ-O)(μ-S)(μ-py)}[63,64] where L = OO′-di-iso-propyl phosphorodithioate). Possibly, in solution the large cone angle swept out by the ONep ligand prevents coordination of pyridine to the monomeric species but upon crystallization to the dimer, the ONep ligands become "locked-in" with only enough room to allow the "crevice" pyridine to bind.

For **2a** and **3a** a trinuclear species was solved with a bridging μ_3-O and surprising μ_3-OBu^t ligand. The oxo is most likely due to adventitious water in the "dry" pyridine or from the reduction of the ONep upon heating. However, attempts to rationalize the formation of an OBu^t ligand from the decomposition of the ONep ligands could not be formulated. This led us to believe that the homoleptic structure was *not* correct, and one OBu^t is present along with eight ONep ligands. Analyses of the metrical data for **2a** or **3a** are consistent with each other (Table 2) and do not reveal the OBu^t. The FTIR, elemental analyses, and BeD-XRD data of **2** and **3**, do not reveal its presence either, since the OBu^t ligand has an identical construct present in the ONep and is present in

(61) Bowmaker, G. A.; Effendy; Harvey, P. J.; Healy, P. C.; Skelton, B. W.; White, A. H. *J. Chem. Soc., Dalton Trans.* **1996**, 2459.

(62) Rabe, G.; Heise, H.; Yap, G. P. A.; Liable-Sands, L. M.; Guzei, I. A.; Rheingold, A. L. *Inorg. Chem.* **1998**, 4235.

(63) Drew, M. G. B.; Mitchell, P. C. H.; Read, A. R. *Chem. Commun.* **1982**, 238.

(64) Drew, M. G. B.; Mitchell, P. C. H.; Read, A. R. *J. Chem. Soc., Dalton Trans.* **1983**, 649.

Table 2. Selected Metrical Data for **1**[33]−**3a**

|	**1**[33]	**1a**	**1b**	**2**	**2a**	**3**	**3a**
				Dist (Å)			
M---M	3.225	3.234(2)	av 3.063	3.2481(11)	3.2243(7)	3.2035(7)	3.1984(7)
M−OR	av 1.791	av 1.819	av 1.773	av 1.992	av 1.933	av 1.976	av 1.926
M−(μ-OR)	av 2.036	av 2.050	av 2.012	av 2.210	2.170(2)	av 2.186	2.150(3)
M−N		2.532(8)					
M−(μ-O)			av 1.834				
M−(μ_3-O)			av 1.977		2.0988(18)		2.086(3)
				Angles (deg)			
(OR)−M−(OR)	av 102.14	av 98.897		av 94.60	100.06(12)	av 96.67	100.10(17)
M−(μ-OR)−M	av 104.69	104.09(13)	100.88	av 94.51	95.93(9)	av 94.20	96.17(14)
M−(μ-O)−M			105.06				
M−(μ_3-O)−M			111.863		100.37(11)		100.11(17)
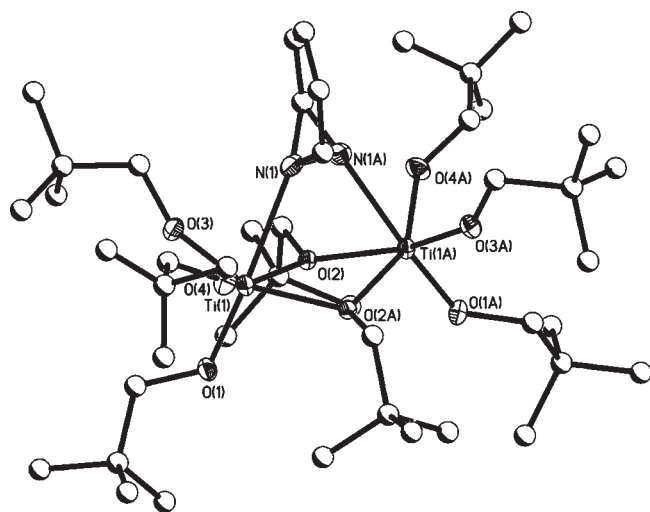
Figure 4. Structure plot of **1a**. Thermal ellipsoids drawn at the 30% level.
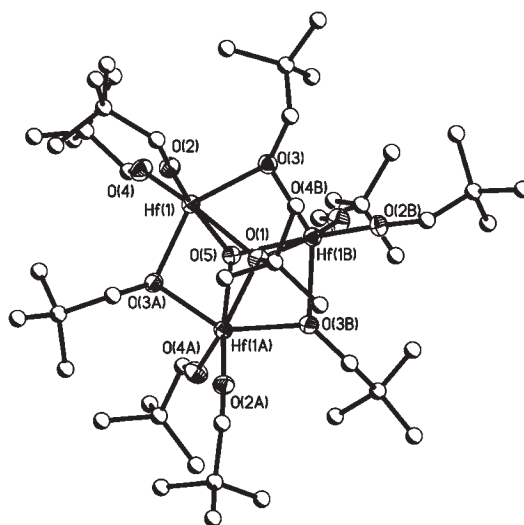

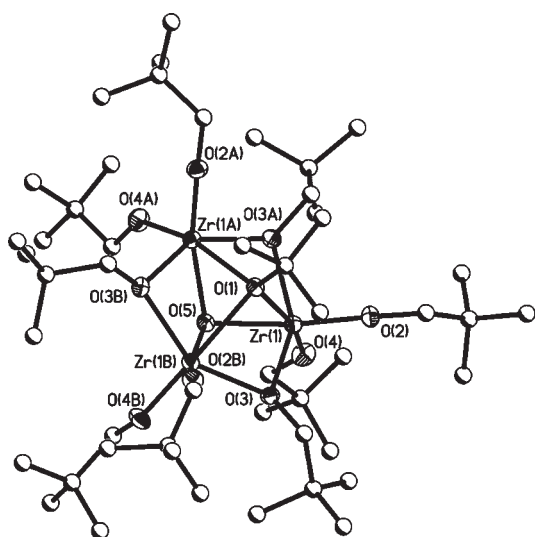**Figure 6.** Structure plot of **3a**. Thermal ellipsoids drawn at the 30% level.

Figure 5. Structure plot of **2a**. Thermal ellipsoids drawn at the 30% level.

a 1:9 ratio. Therefore, crystals of **2** or **3** from CHCl$_3$ were redissolved in tol-d_8 and the ^{1}H and ^{13}C NMR spectra collected. From the crystal structure, three types of ONep ligands would be expected (bridging, terminal and HONep).

Table 3. Properties of Nanomaterials Produced under Different pH Conditions Using **1**−**3** as Precursors

precursor		low (HI)	neutral (H$_2$O)	high (KOH)
1(Ti)	label	**1 nA**	**1 nN**	**1nB**
	phase	rutile syn/ brookite	anatase	anatase
	shape	rod	square - rod	rod
	AR^a	4−5	1	6−8
2(Zr)	label	**2 nA**	**2 nN**	**2nB**
	phase	baddeleyte syn	ZrO$_2$/baddeleyite	baddeleyite
	shape	rods	square - dot	rods - square
	AR	7−8	1	1−3
3(Hf)	label	**3 nA**	**3 nN**	**3nB**
	phase	hafnium oxide	hafnium oxide	hafnium oxide
	shape	rod	square	square
	AR	7−8	1	1

^{a} AR = Aspect ratio estimated from TEM images.

The spectra of **2** and **3** appear to be very similar with three sharp singlets noted in an ratios of 14.0/5.8/62.6 (**2**) and 14.0/8.4/67.5 (**3**). If there is one OBu^t per dinuclear species as observed for **2a** and **3a**, then the expected ratio would be 14.0/9.0/63.0, which is consistent with the observed spectral integrations noted above. Therefore, these resonances
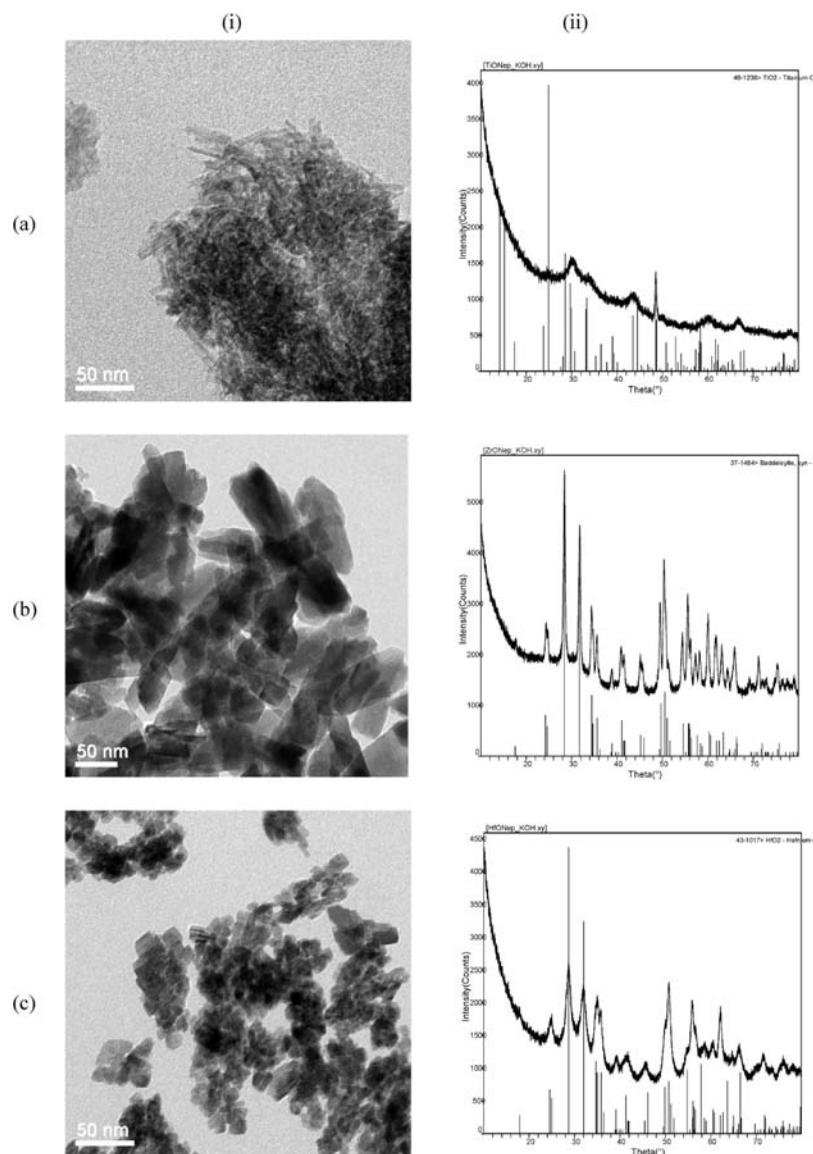
Figure 7. *column* (i) TEM and (ii) PXRD of nanomaterials generated from (10 M) KOH and *row* (a) **1**, (b) **2**, and (c) **3**.

correspond to the ONep methylene, OBu^t methyl, and the ONep methyl proton resonances. The ^{13}C of both also confirm the presence of the OBu^t.

From these data, the real structures of **2** and **3** must be a dinuclear species with a OBu^t and H$^+$ disordered over the 9 ONep sites. The same general structure arrangement of the carbons and the division of the OBu^t by 9, makes the metrical data from the single crystal structure solution for the protons of the ONep and carbons of the OBu^t ligands look strikingly similar. Therefore, we have formulated the general formula of these compounds as {[H][(μ-ONep)$_3$M$_2$(ONep)$_5$(OBu^t)]} M = Zr (**2**) and Hf (**3**).

Nanoparticles. The reproducible production of controlled ceramic nanomaterials from "seeded" growth methods can be problematic. This is due to a number of issues including variations in the "nanoseed" materials (i.e., size or shape) that lead to differences in the growth nuclei and ultimately polydispersed nanoparticles. In contrast, using well-defined precursors that are similar in structure (dinuclear with bridging ONep ligands), and construction (i.e., **1–3**), we reasoned that more uniform

growth nuclei would be generated leading to a better understanding of the cation influences on the final nanomaterials produced. Recently, we investigated the morphological changes wrought from the solvothermal (SOLVO) growth of TiO$_2$ nanoseeds under basic (10 M KOH) and acidic (halide acid: conc. HX (pK_a: HCl = −7 < HBr = −9 < HI = −11) conditions.[1] Ultimately from a scoping study, the hydroiodic acid [(aq) HI] solvent systems at low precursor (**1–3**) concentrations, yielded the most consistent nanomaterials and was therefore employed in this study (see Supporting Information).

Therefore, this route was used to produce nanomaterials using the structurally similar congeners **1–3** in the same basic and acidic systems with an additional neutral SOLVO preparative route, which was not previously useful for the "nanoseed" methodology. The nanoparticles will be referred to according to their precursor number followed by a "*n*" for nanoparticle and either an "A" for acidic, "N" for neutral, or "B" for basic (i.e., nanoparticles generated from **1** in HI would be referred to as "**1nA**"). Data concerning the nanomaterials
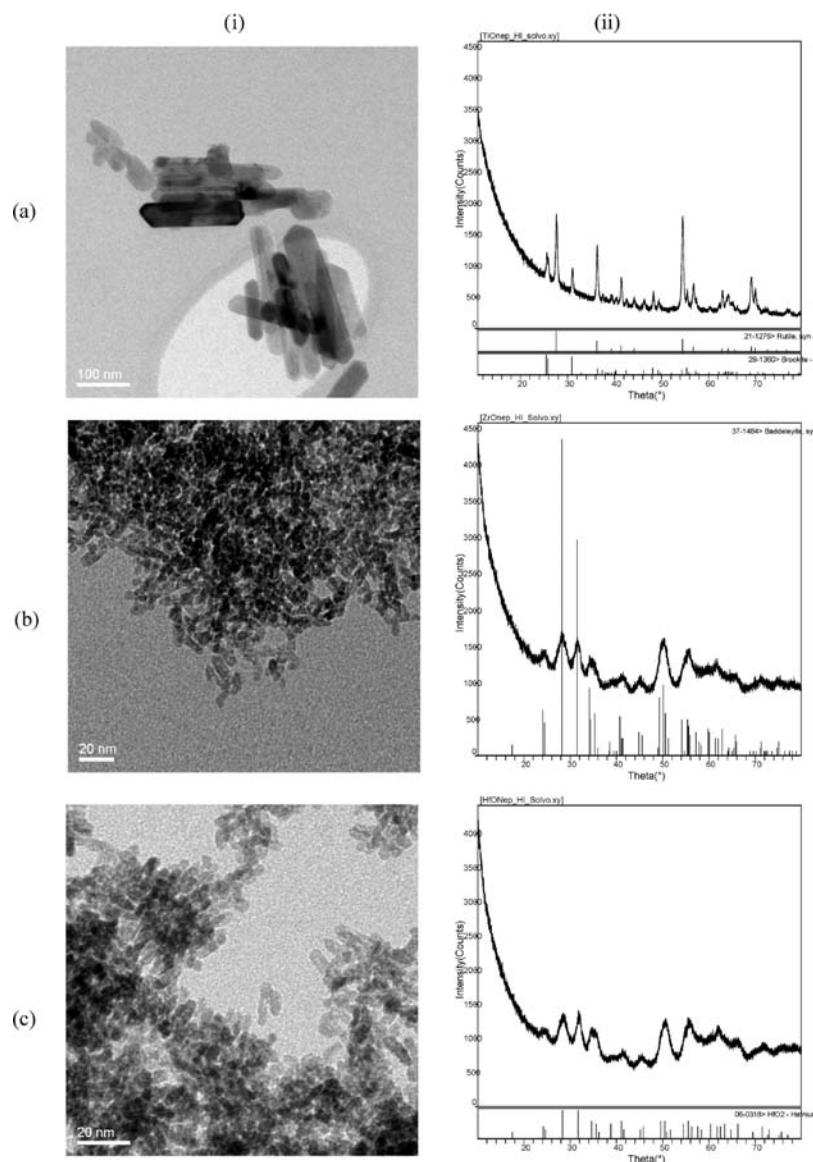
Figure 8. *column* (i) TEM and (ii) PXRD of nanomaterials generated from (aq)HI and *row* (a) **1**, (b) **2**, and (c) **3**.

generated from **1**−**3** are tabulated in Table 3. TEM images as well as the PXRD patterns can be found in Figures 7, 8, and 9 (i and ii) for basic, acid, and neutral conditions, respectively for **1**−**3**.

Basic Conditions. Previously, all processing (SOLVO, SPPT, or hybrid) conditions we investigated that employed TiO_2 "nanoseeds" under basic conditions (10 M KOH) yielded β-phase or TiO_2−B (JCPDS card 00-046-1238) nanowires of different thicknesses.[1] In contrast, the products isolated from **1** (**1nB**) formed short rods of TiO_2−B around 50 nm in length with an ~15−20 nm width [Figure 7a (i and ii)]. In some instances longer rods were noted but typically these were shorter than 150 nm. These short thin rods may have formed because of the instantaneous decomposition of the molecular precursor which yields a nucleation shower of growth nuclei. This leads to numerous growth sites that rapidly consume the precursor feedstock yielding many nanowires that are smaller and thinner than seeded growth systems. This is because for the "nanoseeds" TiO_2 system, the particles are slowly dissolved in the 10 M KOH, leading to slow

elongated growth processes (the original preparation took 3−7 days to finalize wire growth).[1] Again, the starting nuclei of **1b** in comparison to the "nanoseeds" of rutile TiO_2, show the variations that the starting precursor approach can impart.

The initial image of the **2nB** materials generated using **2** under basic conditions, appear as short rods of baddeleyite [Figure 7b(i and ii)]; however, upon closer inspection, the rods are aligned squares and rods that vary in size but are substantially larger than the **1nB** materials. Similar nanomaterials were expected for the **3nB** because of the *iso*-structral nature of the starting precursors. Nanosquares of HfO_2 were observed as seen in Figure 7c-(i and ii). Interestingly, these are substantially smaller with an ~10 nm edge length predominantly observed. From these dinuclear compounds, the cubes noted for **2nB** were the largest in size, followed by the **3nB** cubes, and then the **1nB** nanorods.

Acidic Conditions. There are only a handful of studies that investigate the acidification of TiO_2 for nanoparticle production and these only utilize a catalytic amount of
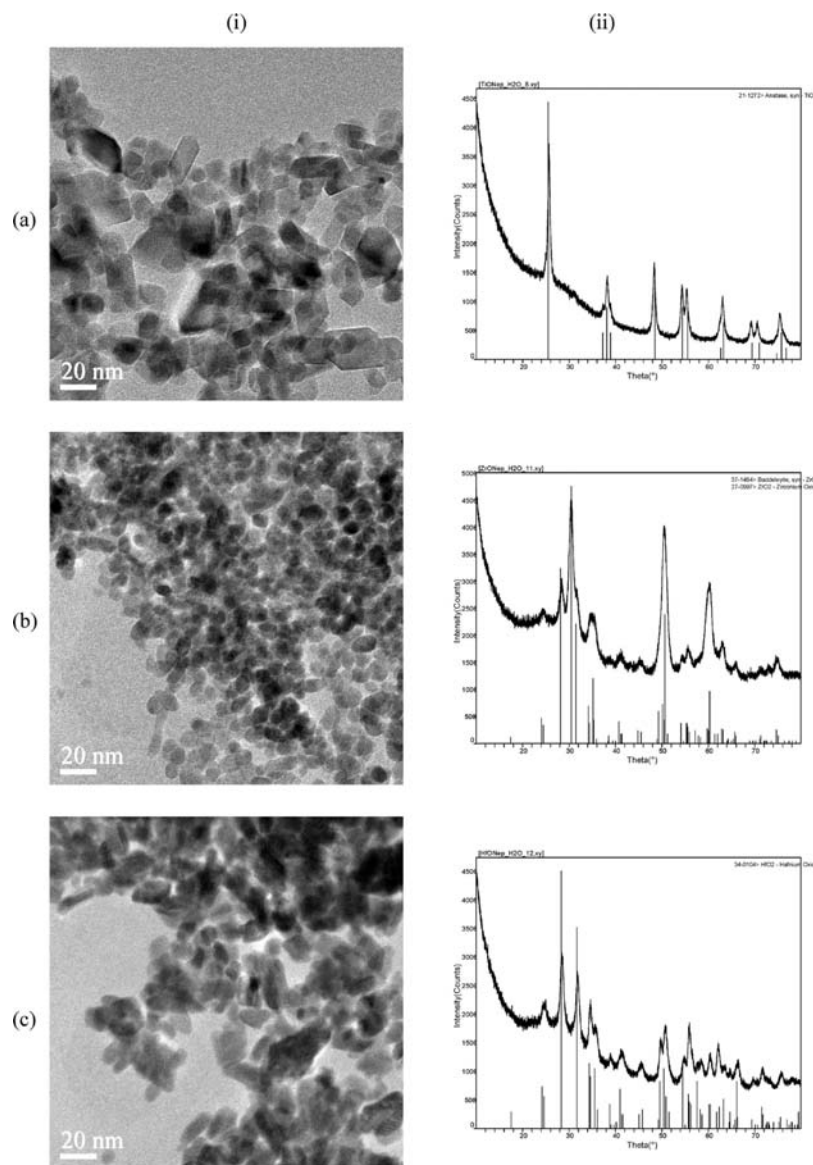
(i)   (ii)

Figure 9. *column* (i) TEM and (ii) PXRD of nanomaterials generated from H$_2$O and *row* (a) **1**, (b) **2**, and (c) **3**.

hydrochloric acid.[65−74] Besides our previous report,[1] we are not aware of any reports that employ the acidic solutions employed here utilizing TiO$_2$, ZrO$_2$, or HfO$_2$ nanoseeds. This is most likely due to the fact that TiO$_2$ is considered insoluble in these media and few commercially available ZrO$_2$ or HfO$_2$ are readily available.[1]

(65) Finnegan, M. P.; Zhang, H.; Banfield, J. F. *J. Phys. Chem. C* **2007**, *111*, 1962.
(66) Penn, R. L.; Banfield, J. F. *Geochim. Cosmochim. Acta* **1999**, *63*, 1549.
(67) Sugimoto, T.; Zhou, X.; Muramatsu, A. *J. Colloid Interface Sci.* **2003**, *259*, 53.
(68) Zaban, A.; Aruna, S. T.; Tirosh, S.; Gregg, B. A.; Mastai, Y. *J. Phys. Chem. B* **2000**, *104*, 4130.
(69) Roy, S. C.; Paulose, M.; Grimes, C. A. *Biomaterials* **2007**, *28*, 4667.
(70) Bright, E.; Readey, D. W. *J. Am. Ceram. Soc.* **1987**, *70*, 900.
(71) Schmuki, P.; Bauer, S.; Kleber, S. *Electrochem. Commun.* **2006**, *8*, 1321.
(72) Wu, G.; Wang, J.; Thomas, D. F.; Chen, A. *Langmuir* **2008**, *24* 3503.
(73) Aruna, S. T.; Tirosh, S.; Zaban, A. *J. Mater. Chem.* **2000**, *10*, 2388.
(74) Lan, Y.; Gao, X. D.; Zhu, H.; Zheng, Z.; Yan, T.; Wu, F.; Ringer, S. P.; Song, D. *Adv. Funct. Mater.* **2005**, *15*, 1310.

Since solubility would be less of an issue (at least pre-liminarily) for the molecular precursors, an investigation of equimolar amounts of **1−3** that were independently added to 10 mL of H$_2$O in a Teflon lined Parr digestion bomb was undertaken. This mixture was then topped off with 10 mL of HI, appropriately sealed, and heated. Diluted concentrated HI was selected for study since it yielded the most uniform complex morphologies from our previous scoping studies (see Supporting Information). The TEM and PXRD of the resultant powders isolated after 24 h at elevated temperatures are shown in Figure 8 (i) and (ii), respectively. Nanorods were noted for each sample investigated. For **1nA**, the rods had aspect ratios (AR) of ~4 forming a mixture of phases: brookite (JCPDS card 00-029-1360; minor) and rutile (JCPDS card 00-021-1276; major). The observance of the high temperature tetra-gonal rutile is not unexpected since it is the most common and stable phase of TiO$_2$. The unusual appearance of the orthorhombic brookite most likely is due to the decom-position of the rutile nanoparticles and further studies to
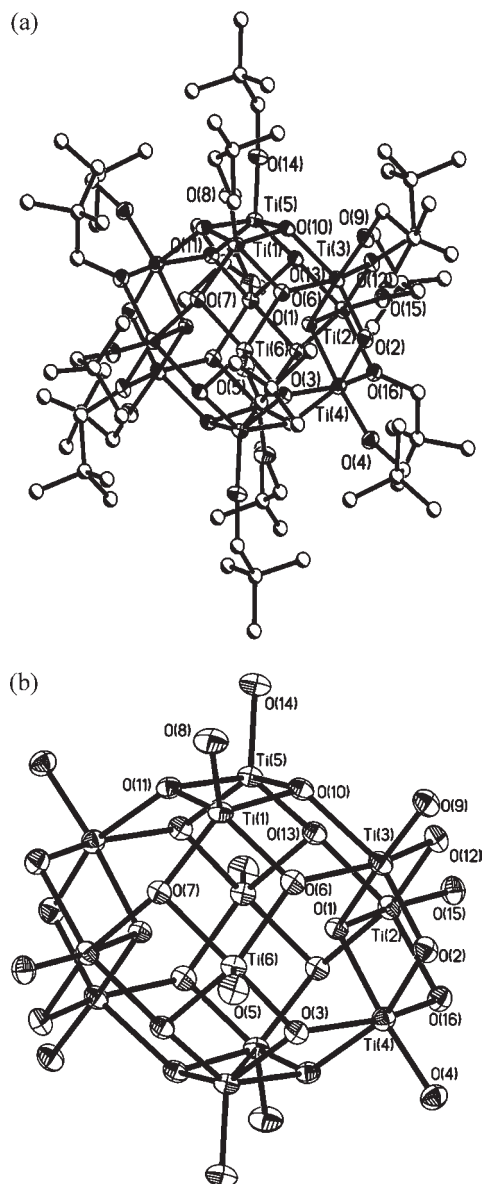
Figure 10. Structure plot of **1b**. Thermal ellipsoids drawn at the 30% level; (a) full structure and (b) central core.

understand and exploit this phenomenon are underway. The TEM images of the nanomaterials generated from **2** and **3** under identical conditions are shown in Figure 8 b(i) and c(i), respectively. The PXRD patterns indicated that the baddelyite [JCPDS card 00-037-1484; Figure 8b(ii)] and hafnium oxide [JCPDS card 00-006-0318; Figure 8c(ii)] nanorods of **2nA** and **3nA**, respectively were much smaller and lower in AR than noted for the **1nA** materials. The **1nA** rods formed vary considerably from the squares noted for anatase TiO_2 nanoseed study but are similar to those formed using rutile TiO_2 nanoseeds.[1] The formation of rods is not unexpected since acicular crystals are often noted for naturally occurring minerals of rutile.

Neutral Conditions. The simple hydrothermal processing of **1−3** was also undertaken, and the final products are shown in Figure 9 a−c (i), respectively. The TEM images of **1nN** shown in Figure 9a(i) reveal square and parallel-pipped, anatase-phased nanomaterials [Figure 9a(ii)] had been formed. The size of the particles is varied, but the

majority range from 20−50 nm. In contrast, the **2nN** nanomaterials are much smaller, consisting of ∼10 nm dots of the baddeleyite and the zirconium oxide [JCPDS card 00-027-0997, see Figure 9b(i)]. The monoclinic baddeleyite phase is stable up to 1200 °C where it then converts to the tetragonal and ultimately the cubic phase as the temperature is increased [Figure 9b(ii)]. However, when non-equilibrium processes are used that form high surface area materials, more phases than the stable monoclinic species may be formed.[75] Therefore, the two phases observed here are either a result of co-crystallization because of the high surface area nanomaterials forming in a non-equilibrium situation or the low temperature monoclinic baddeleyite was only partially transformed into the higher temperature cubic ZrO_2 phase under the conditions noted. Longer processing times and different temperatures are being explored to understand the mixed phase production. The **3nN** species [Figure 9c(i)] were found to be larger than the **2nN** but smaller than the **1nN** materials. The hafnium oxide [Figure 9c(ii)] particles resemble ∼20 nm rod-like species with some dots present but not as plentiful as the dots noted for **2nN**. The elongation of the Hf particles over those of the Zr are not fully understood but can only be an effect of the metal center (i.e., variations in hydrolysis susceptibility Zr < Hf).[76] In particular, the formation of a single phase as noted for the Hf system, would favor formation of more uniform particles.

Hydrolysis of Precursors. Overall, the nanomaterials generated with **1−3**, when compared to the seeded growth system,[1] demonstrated significant changes in the final morphologies produced. Interestingly, the expected improvement in the monodispersity was not observed. This is believed to be due to the properties associated with the cation's hydrolysis behavior, since each system involves an aqueous based solution. Our initial efforts focused on identifying the hydrolysis product of **1−3**, which would be considered the basic building blocks of the nanomaterials ultimately produced.

The reaction was simplified to investigate the hydrolysis of **1−3** over a very short time (1 equiv of H_2O/ toluene was added to a solution of **1−3** in toluene and stirred for 10 min). After the volatile component was removed in vacuo the resulting white powders were subsequently crystallized from toluene, which proved to be $[Ti_6(\mu_3\text{-}O)_7(\mu\text{-}O)(\mu\text{-}ONep)_2(ONep)_6]_2$ (**1b**, Figure 10) and the previously discussed $\{(\mu_3\text{-}O)(\mu_3\text{-}OBu^t)[(\mu\text{-}ONep)M(ONep)_2]_3\}$ M = Zr (**2a**) and Hf (**3a**). The structure of **1b** is similar to that reported previously for the hydrolysis[51] or esterification[77,78] of the $Ti(OCHMe_2)_4$. The dodecamer adopts a pseudo-C_{2h} symmetry forming a triangular gyrobicupola consisting of a mixture of 5- and 6-coordinated Ti metal centers. This ball shaped structure is ∼6.5 Å across [Ti(5)---Ti(5a)] omitting the ONep pendant chains and must be considered a fundamental building block of TiO_2 materials. The similarity between the direct hydrolysis product and those obtained from py (**2a** and **3a**) must be related to the high temperatures

(75) Armelao, L.; Bertagnolli, H.; Gross, S.; Krishnan, V.; Lavrencic-Stangar, U.; Muller, K.; Orel, B.; Srinivasan, G.; Tondello, E.; Zattin, A. *J. Mater. Chem.* **2005**, *15*, 1954.
(76) Pershina, V. *J. Nucl. Rad. Sci.* **2002**, *3*, 137.
(77) Stenou, N.; Robert, F.; Boubekeur, K.; Ribot, F.; Sanchez, C. *Inorg. Chim. Acta* **1998**, *279*, 144.
(78) Day, V. W.; Eberspacher, T. A.; Klemperer, W. G.; Park, C. W. *J. Am. Chem. Soc.* **1993**, *115*, 8469.

required to dissolve **2** and **3** in this solvent and adventitious water present in the "anhydrous" py. Therefore, the triangular shaped **2a** and **3a** constitute the start of the hydrolysis and may be considered the first of many steps leading to large oligomers as observed for **1b**.

The shape and size of the precursor has been previously shown to directly impact the final morphology observed in a number of nanoparticle systems.[79−82] Therefore, the larger structure noted for **1b** would be expected to yield much larger particles than those observed from the trinuclear **2a** and **3a** for systems driven by the hydrolysis behavior of the precursor. For both the acidic and neutral pH solutions investigated this was the case (**1nA** > **3nA** ~ **2nA** and **1nN** > **3nN** ~ **2nN**). Interestingly, this was not the case for the basic solution, where **2nB** > **3nB** > **1nB**. Because of these inconsistencies and the fact that even though similar nucleation seeds are available for **2** and **3** (i. e., **2a** and **3a**), hydrolysis cannot be the only driving factor. The next parameter that must be considered is the solubility of the in situ generated "MO$_2$" growth particles in the medium used. Because of the limited information available for the heavier congeners at the different pH levels studied here, more studies are necessary.

Summary and Conclusions

The dinuclear Group 4 *neo*-pentoxide species have been isolated as **1−3**. The heavier cations were found to be novel *iso*-structural complexes with the presence of a OBu^t ligand and a H disordered over the entire molecule. Upon dissolution in pyridine an unusual "crevice" structure was noted for **1a**, whereas **2** and **3** formed an oxo- compound (**2a** and **3a**) where the OBu^t could be specifically identified. Direct hydrolysis studies of **1−3** lead to the isolation of the dodecamer

compound **1b** for **1** but **2a** and **3a** were again isolated for **2** and **3**, respectively. Because of their structural similarities (dinuclear with bridging ONep ligands), compounds **1−3** were used to explore the effect that the cation from the isomorphic species have on the final nanomaterials generated using a SOLVO approach at different pH levels: acidic [(aq)HI], neutral [H$_2$O)], and basic [(aq)KOH]. For acidic routes, small nanorods were formed, neutral solutions led to nanosquares, and basic preparations yielded larger nanorods. For Ti, a variety of phases formed based on the pH whereas Zr typically formed baddeleyite and Hf formed HfO$_2$. The nanomorphologies isolated here appear to be substantially different from the seeded growth approach; however, significant improvements in the distribution of size and shape were not noted. The hydrolysis products (**1b**, **2a**, **3a**) appear to play a role in directing the size of the final nanomaterials; investigation of the solubility of the MO$_2$ in these systems must be explored to fully understand the final morphologies attained. Additionally, lower processing temperatures are being explored to exploit the lower thermal stability of these precursors (**1−3**).

Supporting Information Available: BeD-XRD (calc'd and experimental) of **1−3** along with scoping study (PXRD, TEM) of **1−3** in HX (X = Cl, Br, I) at low medium and high concentrations. This material is available free of charge via the Internet at http://pubs.acs.org. The crystal structures of **1a−3a** have been deposited at the Cambridge Crystallographic Data Centre and allocated the deposition numbers CCDC 775237−775242, respectively.

(79) Boyle, T. J.; Hernandez-Sanchez, B. A.; Baros, C. M.; Rodriguez, M. A.; Brewer, L. N. *Chem. Mater*. **2007**, *19*, 2016.

(80) Boyle, T. J.; Bunge, S. D.; Alam, T. M.; Holland, G. P.; Headley, T. J.; Avilucea, G. *Inorg. Chem*. **2005**, *44*, 1309.

(81) Boyle, T. J.; Bunge, S. D.; Andrews, N. L.; Matzen, L. E.; Sieg, K.; Rodriguez, M. A.; Headley, T. J. *Chem. Mater*. **2004**, *16*, 3279.

(82) Boyle, T. J.; Tribby, L. J.; Ottley, L. A. M.; San, S. M. *Eur*. *J. Inorg. Chem*. **2009**, *36*, 5550.